Gravitational lens effect of a holonomy corrected Schwarzschild black hole

Ednaldo L. B. Junior[1,*] Francisco S. N. Lobo[2,3,†] Manuel E. Rodrigues[4,5,‡] and Henrique A. Vieira[4,§]

[1]*Faculdade de Física., Universidade Federal do Pará,*
Campus Universitário de Tucuruí, CEP: 68464-000, Tucuruí, Pará, Brazil
[2]*Instituto de Astrofísica e Ciências do Espaço, Faculdade de Ciências da Universidade de Lisboa,*
Edifício C8, Campo Grande, P-1749-016 Lisbon, Portugal
[3]*Departamento de Física, Faculdade de Ciências da Universidade de Lisboa,*
Edifício C8, Campo Grande, P-1749-016 Lisbon, Portugal
[4]*Faculdade de Física, Programa de Pós-Graduação em Física,*
Universidade Federal do Pará, 66075-110, Belém, Pará, Brazill
[5]*Faculdade de Ciências Exatas e Tecnologia, Universidade Federal do Pará,*
Campus Universitário de Abaetetuba, 68440-000, Abaetetuba, Pará, Brazil

In this paper we study the gravitational lensing effect for the Schwarzschild solution with holonomy corrections. We use two types of approximation methods to calculate the deflection angle, namely the weak and strong field limits. For the first method, we calculate the deflection angle up to the fifth order of approximation and show the influence of the parameter λ (in terms of loop quantum gravity) on it. In addition, we construct expressions for the magnification, the position of the lensed images and the time delay as functions of the coefficients from the deflection angle expansion. We find that λ increases the deflection angle. In the strong field limit, we use a logarithmic approximation to compute the deflection angle. We then write four observables, in terms of the coefficients b_1, b_2, and u_m, namely: the asymptotic position approached by a set of images θ_∞, the distance between the first image and the others s, the ratio between the flux of the first image and the flux of all other images r_m, and the time delay between two photons $\Delta T_{2,1}$. We then use the experimental data of the black hole Sagittarius $A^\star$ and calculate the observables and the coefficients of the logarithmic expansion. We find that the parameter λ increases the deflection angle, the separation between the lensed images and the delay time between them. In contrast, it decreases the brightness of the first image compared to the others.

I. INTRODUCTION

Shortly after Einstein published the field equations of general relativity [1], Karl Schwarzschild [2] proposed an exact solution to these equations, which became known as the Schwarzschild black hole [3]. The current definition of these bodies is a region of spacetime covered by an event horizon from which not even light can escape. Initially, black holes were discredited and many argued that they were just a mathematical solution with no relation to reality. However, they gained notoriety in the 1960s with the discovery of compact objects and more recently with the first image of the shadow of what is believed to be a supermassive black hole [4–9]. Over the years, many other exact solutions have appeared, such as those of Reissner-Nordström and Kerr [10], but like the Schwarzschild

geometry, they suffered from a peculiarity that troubled the scientific community, i.e., the existence of a singularity. A curvature singularity is a sudden endpoint in the geodesic equations at which quantities such as the density of matter become infinite. In fact, the notion of geodesic completeness essentially resides at the root of the singularity theorems [11] and is considered as a key element to determine the presence of a spacetime singularity [12].

The main focus of physicists attempting to eliminate the singularity is the development of a theory of quantum gravity. Initial attempts date back to the middle of the last century [13], but we still have neither a satisfactory theory nor experimental data on the quantum aspects of gravity [14]. For instance, we refer the reader to [15,16] and references therein to get a compilation of modern quantum gravity, including its challenges and advances. Alternatively to searching for a complete quantum description of gravitation there is the possibility to describe some phenomena at low energy scales (compared to the Plack scale) [17–19]. Through these models it is also possible to find corrections from gravitation to quantum electrodynamics [20–22] and

*ednaldobarrosjr@gmail.com
†fslobo@ciencias.ulisboa.pt
‡esialg@gmail.com
§henriquefisica2017@gmail.com

024004-1

to quantum chromodynamics (QCD) [23]. Another interesting point is the influence of quantum gravitation on dark matter [24,25]. Among the various effective theories, the so-called loop quantum gravity (LQG) has gained notoriety. In cosmology, LQG has been used in the creation of cosmological models without singularity [26–28], explanation of the big bang [29,30], and other effects [31,32]. In black hole physics, Ashtekar and collaborators [33] used the LQG formalism and obtained a new derivation for the Bekenstein-Hawking formula, Vakili [34] use the Schwarzschild metric as background geometry in the framework of classical polymerization and showed that its energy-momentum tensor has the features of dark energy. Several other papers have also studied LQG corrections to the Schwarzschild solution [35–38]. Recently, Alonso-Bardaji, Brizuela and Vera [39,40] used a canonical transformation and a linear combination of the general relativity constraints to propose a black hole model consisting of an LQG correction to the Schwarzschild solution. It is an anomaly-free model described by the following metric

$$ds^2 = -A(r)dt^2 + \left[\left(1 - \frac{l}{r} \right) A(r) \right]^{-1} dr^2$$
$$+ r^2 (d\theta^2 + \sin^2\theta d\phi^2 \sin), \quad (1)$$

where $A(r) = 1 - 2m/r$ is the usual Schwarzschild metric function, and l is a new scale length defined by $l := 2m\lambda^2/(1 + \lambda^2)$, where λ is called the polymerization constant and provides the holonomy correction information. For $m > 0$, this solution is asymptotically flat and contains a globally hyperbolic black hole or white hole region with a minimal space-like hypersurface replacing the original singularity. The full information on the event horizons, Penrose diagram, and spacetime structure associated with this model can be found in the original papers mentioned earlier. In addition, it was show in [41] (a work focused on quasinormal modes) that perturbations become less damped as we increase the LQG parameter λ.

The purpose of this work is to study the light deflection properties of the solution present in [39,40]. The deflection of light rays by a massive body can produce a widely known effect, namely, gravitational lensing. At first, physicists, including Einstein, believed that this effect could be observed only in experiments such as the one in 1919 [42]. At that time, astronomers could measure the deflection angle caused by the Sun during a solar eclipse [43]. In fact, this kind of observation is possible only with the Sun. This reasoning began to change with the pioneering ideas of Fritz Zwicky, who proposed that we can observe lensing effects caused by galaxies and even clusters of galaxies. For a more detailed overview of the early measurements and theoretical proposals on this topic, see, for example, [44–47] and the references therein. Recent developments related to this effect can be divided into two groups: strong lensing and microlensing [44].

Strong lensing is related to measurements of galaxies and clusters of galaxies and has gained notoriety since the discovery of the accelerating expansion of the Universe [48,49]. The reason is that we do not know why the Universe is expanding, and a popular approach to explain this behavior is the presence of an exotic cosmic fluid denoted as dark energy [50]. Although there is no direct measurement of dark energy, we have tempting evidence for its existence [51], where the weak gravitational lensing effect plays an important role in these measurements [52]. Much work has been done in the literature, for instance, Bartelmann and Schneider [53] have shown how to obtain the deflection angle within these limits; Holz and Wald [54] presented a similar method for inhomogeneous universes; Lewis and Challinor [55] commented on how the weak lensing effects affect the cosmic microwave background; and Ghaffarnejad and Niad [56] calculated this effect considering a Bardeen black hole. For an overview of these and other methods using weak lensing, we refer the reader to [57].

Another motivation arising from strong lensing is the possibility of testing general relativity in a strong gravitational field (so far it has been tested only for weak fields). Bozza [58] proposed a way to calculate the deflection angle by a logarithmic expansion. Later, Bozza and Mancini applied this formalist to Sgr A* to describe how to observe real black holes with GRAVITY [59]. Pietroni and Bozza, also considering Sgr A*, commented on the effect of gravitational lensing on stellar orbit reconstruction [60]. Naoki Tsukamoto reproduced Bozza's formalism considering a slightly unstable photon sphere [61], then applied it to Simpson-Visser spacetime [62] and to a Reissner-Nordström naked singularity [63]. J. Zhang and Y. Xie later considered a black-bounce- Reissner-Nordström solution [64]. Advances in this field is not limited to the theoretical realm, but there are also recent attempts to observe this effect for supermassive black holes [65,66]. Microlensing is the measurement of the collective magnification of various images; in the case of stars, the observation may take months or even years [44]. This type of measurement can be used in the detection of bodies that do not emit light, such as planets [67,68] or black holes [69]; and also helps in the study of binary star systems [70,71]. In addition, there are several other ways to apply gravitational lensing that are still in the theoretical realm. In [72] the authors claim that it can be used as a distance estimator, and in [73–75] a formalism for testing gravitational theories using lenses through compact objects was proposed. In [76], gravitational lensing in the Kehagias-Sfetsos space-time [77], emerging in the framework of Hořava-Lifshitz gravity, has also been analyzed. In [78], light bending serves as constraints on axionic fuzzy dark matter.

As mentioned above, in this work we will study the gravitational lensing effect for the Schwarzschild solution with holonomy corrections. We will consider two types of

approximations, namely strong and weak lensing. This paper is organized as follows: In Sec. II, we will briefly discuss the main aspects of the weak lensing system and then apply it to the above solutions. In Sec. III; we will calculate again the first term of the weak field expansion using the Gauss-Bonnet theorem, and in Sec. IV we repeat the same procedure as in the previous section, now considering strong lensing. In Sec. V we numerically calculated the observavaies using data from the black hole at the center of our Galaxy. In Sec. VI we discussed an extension of the photon surface concept to the case of massive particles. In Sec. VII, we draw our conclusions. We will use the metric signature $(-, +, +, +)$ in this paper. Also, unless otherwise stated, we will use geometrized units with $G = c = 1$.

II. WEAK GRAVITATIONAL LENSING

A. Setting the stage

In this section, we compute the deflection angle and the observable (image position and magnification) for the Schwarzschild solution with holonomy corrections, given by Eq. (1), in the weak field limit. In this regime, we assume that both the source and the observer are very far from the lens and the light rays are only slightly distorted by the lens. Formally, we can define the weak field limit as follows:

(i) The gravitational lens is compact, static, and spherically symmetric, with an asymptotically flat spacetime geometry far away from the lens. The spacetime is vacuum outside the lens and flat in the absence of the lens.

(ii) The observer and the source lie in the asymptotically flat regime of the spacetime.

(iii) The distance scale is much larger than the mass scale, i.e.,

$$\frac{m}{r_0} \ll 1, \qquad \frac{m}{u} \ll 1, \qquad (2)$$

where r_0 is the distance of closest approach to the lens and u is the impact parameter.

To start with, we show in Fig. 1 the usual scheme of light deflection, from which we derive the lens equation as

$$\tan\beta = \tan\vartheta - D(\tan\vartheta + \tan(\alpha - \theta)), \qquad (3)$$

where β and θ are the angular position of the source and the lensed images, respectively, and

$$D = \frac{D_{LS}}{D_{OS}} \qquad (4)$$

with $D_{OS} = D_{LS} + D_{OL}$ being the distance between the observer and the source (where D_{LS} and D_{OL} are the distances marked in the figure).
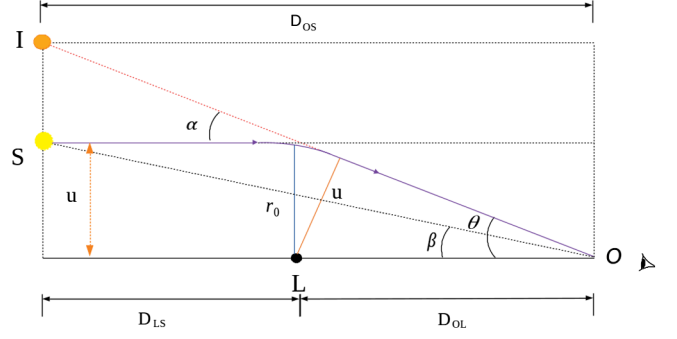

FIG. 1. Simplified schematization of the gravitational lensing phenomenon. The light emitted by the source S is slightly deflected from its original trajectory and arrives at the observer O with an angle θ instead of β. The deflection angle α is the distance between the image I and the actual position of the source. The relevant distances in the figure are: the impact parameter u, the distance of closest approach x_0, the distance from the observer to the lens D_{OL} and the distance from the lens to the source D_{LS}.

In order to calculate the angle α, we first assume a static and spherically symmetric spacetime defined by

$$ds^2 = -A(r)dt^2 + B(r)dr^2 + C(r)d\Omega^2, \qquad (5)$$

where $d\Omega^2$ is the standard unit sphere metric. The deflection angle α is given by [44,79]

$$\alpha(r_0) = 2 \int_{r_0}^{\infty} \frac{1}{C} \sqrt{\frac{AB}{1/u^2 - A/C}} dr - \pi. \qquad (6)$$

The above integral can only be solved analytically for some simple cases. Thus, Keeton and Petters [73] suggested that this result can be approximated by a series of the following form

$$\alpha(u) = \mathcal{A}_1 \left(\frac{m}{u}\right) + \mathcal{A}_2 \left(\frac{m}{u}\right)^2 + \mathcal{A}_3 \left(\frac{m}{u}\right)^3 + \mathcal{O}\left(\frac{m}{u}\right)^4. \qquad (7)$$

Here, the deflection angle is written as a function of the impact parameter u, since it is a gauge invariant variable (while the closest approach distance has a gauge dependence). The $\mathcal{A}_i$ are coefficients to be calculated, which can be simple numbers or depend on a parameter of the solution, such as the charge. It is worth mentioning that this formalism possesses several limitations, which we consider below.

To demonstrate how this formalism works, we will apply it to the Schwarzschild metric. In this case we have

$$A(r) = 1 - \frac{2m}{r},$$
$$B(r) = A(r)^{-1},$$
$$C(r) = r^2. \qquad (8)$$

Substituting these components into (6)

$$\alpha(r_0) = 2 \int_{r_0}^{\infty} \frac{1}{r^2} \frac{dr}{\sqrt{1/u^2 - 1/r^2 + 2m/r^3}} - \pi, \quad (9)$$

to solve this, we first make a coordinate change $x = r_0/r$ and $h = m/r_0$, which leads to the following results

$$\alpha(r_0) = 2 \int_0^1 \frac{dx}{\sqrt{1 - 2h - x^2 + 2hx^3}} - \pi. \quad (10)$$

Here we used that the relation between r_0 and u is

$$u = \sqrt{\frac{C(r_0)}{A(r_0)}}, \quad (11)$$

which in this case becomes

$$u = \frac{r_0}{\sqrt{1 - \frac{2m}{r_0}}}. \quad (12)$$

Now, assuming the weak field regime, i.e. $h \ll 1$, we expand the integrand into a Taylor series and then solve the integral term by term, which provides

$$\alpha(r_0) = 4h + \left(\frac{15\pi}{4} - 4\right)h^2 + \left(\frac{122}{3} - \frac{15\pi}{2}\right)h^3$$
$$+ \left(\frac{3465\pi}{64} - 130\right)h^4 + \left(\frac{7783}{10} - \frac{3465\pi}{16}\right)h^5$$
$$+ \left(\frac{310695\pi}{256} - \frac{21397}{6}\right)h^6 + \mathcal{O}(h)^7. \quad (13)$$

To convert this expression into the form (7) we use Eq. (12) to relate r_0 and u as follows

$$\frac{r_0}{u} = \frac{2}{\sqrt{3}} \cos\left(\frac{1}{3} \cos^{-1}\left(-\frac{3^{3/2}m}{u}\right)\right), \quad (14)$$

then, we can write

$$r_0 = \frac{4m}{u} + \frac{15\pi m^2}{4u^2} + \frac{128m^3}{3u^3} + \frac{3465\pi m^4}{64u^4}$$
$$+ \frac{3584m^5}{5u^5} + \frac{255255\pi m^6}{256u^6} + \mathcal{O}(m^7). \quad (15)$$

Inserting Eq. (15) into Eq. (13), we finally obtain

$$\alpha(u) = 4\frac{m}{u} + \frac{15\pi}{4}\left(\frac{m}{u}\right)^2 + \frac{128}{3}\left(\frac{m}{u}\right)^3 + \frac{3465\pi}{4}\left(\frac{m}{u}\right)^4$$
$$+ \frac{3584}{5}\left(\frac{m}{u}\right)^5 + \frac{255255\pi}{256}\left(\frac{m}{u}\right)^6 + \mathcal{O}\left(\frac{m}{u}\right)^7. \quad (16)$$

Note that with this procedure we obtain Einstein's result, i.e., $\mathcal{A}_1 = 4$, which is twice Newton's result [79]. Here the coefficients $\mathcal{A}_n$ are only numbers, as the solution has only one parameter, namely the mass m.

B. Deflection angle

Now, taking into account the holonomy correction (1), which is given by a change in the length scale

$$l := 2m \frac{\lambda^2}{1 + \lambda^2}, \quad (17)$$

the LQG correction to the Schwarzschild solution (1) is given by

$$A(r) = 1 - \frac{2m}{r},$$
$$B(r) = \frac{1}{(1 - \frac{2m}{r})(1 - \frac{2m\lambda^2}{(\lambda^2+1)r})},$$
$$C(r) = r^2. \quad (18)$$

Thus, Eq. (6) takes the following form

$$\alpha(r_0) = 2 \int_{r_0}^{\infty} \frac{dr}{r^2} \left[\frac{(\lambda^2 + 1)r}{(\lambda^2(r-1) + r)\left(\frac{2m-r}{r^3} - \frac{2m}{r_0^3} + \frac{1}{r_0^2}\right)}\right]^{1/2}. \quad (19)$$

Note that Eq. (12) holds for this model. Now we use the same substitutions as in the previous section, i.e. $x = r_0/r$ and $h = m/r_0$, which leads us to the following results

$$\alpha(r_0) = 2\sqrt{\frac{1}{(2h(x^3 - 1) - x^2 + 1)(1 - \frac{2h\lambda^2 x}{\lambda^2 + 1})}} - \pi. \quad (20)$$

In the weak field regime we have $h \ll 1$ and we can therefore use a Taylor series expansion for the integrand of the above expression in terms of h. So we can calculate the integral term by term, which results in

$$\alpha(r_0) = h^5\left(-\frac{5}{4}(63\pi - 223)\lambda^2 - \frac{3465\pi}{16} + \frac{7783}{10}\right)$$
$$+ h^4\left(\frac{315\pi\lambda^2}{16} - 49\lambda^2 + \frac{3465\pi}{64} - 130\right)$$
$$+ h^3\left(-3(\pi - 5)\lambda^2 - \frac{15\pi}{2} + \frac{122}{3}\right)$$
$$+ h^2\left(\frac{3\pi\lambda^2}{2} + \frac{1}{4}(15\pi - 8(\lambda^2 + 2))\right) + 2h(\lambda^2 + 2). \quad (21)$$
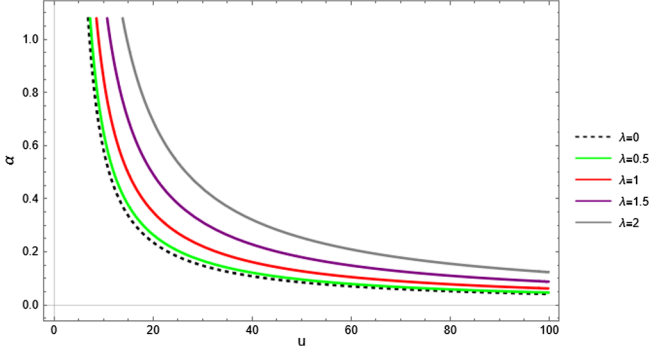
FIG. 2. Graphical representation of the deflection angle, given by the Eq. (22) with the coefficients (23), for the Schwarzschild with holonomy corrections. Here $m = 1$, and $\lambda = 0$ represent the standard Schwarzschild solution.

This gives us an approximation for the deflection angle in powers of m/r_0. To convert this result into an approximation in terms of m/u, we use Eq. (15) and get

$$\alpha(u) = \mathcal{A}_1 \frac{m}{u} + \mathcal{A}_2 \left(\frac{m}{u}\right)^2 + \mathcal{A}_3 \left(\frac{m}{u}\right)^3 + \mathcal{A}_4 \left(\frac{m}{u}\right)^4$$
$$+ \mathcal{A}_5 \left(\frac{m}{u}\right)^5 + \mathcal{O}\left(\frac{m}{u}\right)^6, \quad (22)$$

where

$$\mathcal{A}_1 = 2(\lambda^2 + 2), \qquad \mathcal{A}_2 = \frac{3\pi(2\lambda^2 + 5)}{4},$$

$$\mathcal{A}_3 = \frac{16(3\lambda^2 + 8)}{3}, \qquad \mathcal{A}_4 = \frac{315\pi(4\lambda^2 + 11)}{64},$$

$$\mathcal{A}_5 = \frac{256(5\lambda^2 + 14)}{5}. \quad (23)$$

This result shows that the constant polymerization parameter λ increases the deflection angle. One can easily verify that if $\lambda = 0$, then Eq. (16) is recovered. However, in this case we have $\mathcal{A}_1 \neq 4$, which emphasizes the fact that we are not dealing with classical general relativity. In Fig. 2, we plot α against the impact parameter u.

C. Positions of lensed images

From now on, we use the coefficients of the deflection angle expansion given in Eq. (22) to calculate the following observables: the image position, the magnification and the time delay between the primary and secondary images. First, we change the variables in the lens equation (3) by using the weak Einstein deflection ring radius,

$$\theta_E = \sqrt{\frac{4GmD_{LS}}{c^2 D_{OL} D_{OS}}} = \sqrt{\frac{4mD_{LS}}{D_{OL} D_{OS}}} \quad (24)$$

and we define

$$\beta = \frac{\beta}{\theta_E}, \qquad \theta = \frac{\vartheta}{\theta_E}, \qquad \epsilon = \frac{\tan^{-1}(m/D_{OL})}{\theta_E} = \frac{\theta_E}{4D}. \quad (25)$$

We now assume a solution of the lens equation (3) in the form (the Einstein ring is a natural scale in this context, so we will write all the other quantities involved in ϵ power expansions)

$$\theta = \theta_0 + \theta_1 \epsilon + \theta_2 \epsilon^2 + \theta_3 \epsilon^3 + \mathcal{O}(\epsilon)^4. \quad (26)$$

Then we can write the deflection angle as

$$\alpha = \frac{\mathcal{A}_1}{\theta_0} \epsilon + \frac{\mathcal{A}_2 - \mathcal{A}_1 \theta_1}{\theta_0^2} \epsilon^2 + \frac{1}{\theta_0^3} \left[\mathcal{A}_2 - 2\mathcal{A}_3 \theta_1 \right.$$
$$\left. + \mathcal{A}_1 \left(\frac{8}{3} D^2 \theta_0^4 + \theta_1^2 - \theta_0 \theta_2 \right) \right] \epsilon^3 + \mathcal{O}(\epsilon)^4. \quad (27)$$
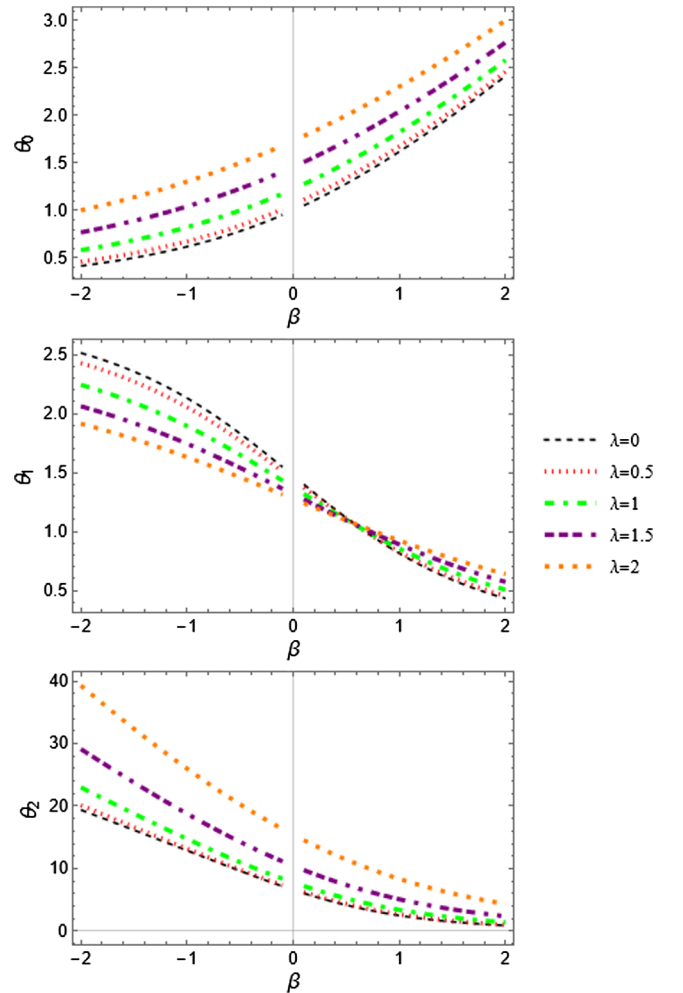

FIG. 3. Graphical representation of the components of the θ expansion, given by the Eq. (30), as a function of the angle β. We have considered $D = 0.01$. We have the positive-parity image when $\beta > 0$ and negative-parity image for $\beta < 0$. We omit the regions with $|\beta| = 0.1$ for obvious physical reasons.

Putting these pieces together, we fix β and solve the lens equation term by term to find the coefficients θ_i [73]. The first one is

$$\theta_0 = \frac{1}{2}\left(\sqrt{\beta^2 + \mathcal{A}_1} + \beta\right). \tag{28}$$

The other coefficients are given in terms of θ_0 and $\mathcal{A}_i$. For the solution considered we have

$$\theta_1 = \frac{3\pi(2\lambda^2 + 5)}{8(2\theta_0^2 + \lambda^2 + 2)}, \tag{29}$$

$$\begin{aligned}
\theta_2 = &\{192\theta_0(2\theta_0^2 + \lambda^2 + 2)^3\}^{-1}\{512D^2[4\theta_0^8(\lambda^2 - 10) + 4\theta_0^6(7\lambda^4 + 16\lambda^2 + 16) + \theta_0^4(7\lambda^6 + 30\lambda^4 + 84\lambda^2 + 88) \\
&+ 4\theta_0^2(3\lambda^4 + 8\lambda^2 + 4) - 4(\lambda^2 + 2)^2] - 1536D\theta_0^2(\lambda^2 + 2)^2(2\theta_0^2 + \lambda^2 + 2)^2 + 256[4\theta_0^4(\lambda^6 + 6\lambda^4 + 18\lambda^2 + 24) \\
&+ \theta_0^2(\lambda^2 + 2)(4\lambda^6 + 24\lambda^4 + 69\lambda^2 + 90) + (\lambda^2 + 2)^2(\lambda^6 + 6\lambda^4 + 18\lambda^2 + 24)] - 27\pi^2(\lambda^2 + 2)(2\lambda^2 + 5)^2\}. \tag{30}
\end{aligned}$$

The first order correction of the position of the images in the order of ϵ is thus

$$\theta = \theta_0 + \frac{3\pi(2\lambda^2 + 5)}{8(2\theta_0^2 + \lambda^2 + 2)}\epsilon + \mathcal{O}(\epsilon)^2. \tag{31}$$

We can see that there is no influence of the λ on the zero order, only from the first upward. In Fig. 3, we represent the coefficients $\theta_{0,1,2}$ as functions of the angle β [the angles defined by Eq. (25)] for different values of λ. We choose $D = 0.01$ inspired by real situations in which $D_{OS} \gg D_{LS}$.

D. Magnifications

The optical magnification μ, how much an image has decreased or increased in apparent size, is defined by

$$\mu = \left[\frac{\sin(\beta)}{\sin(\theta)}\frac{d\beta}{d\theta}\right]^{-1}, \tag{32}$$

at a angular position θ. As before, we can construct a series expansion for the magnification in terms of ϵ

$$\mu = \mu_0 + \mu_1\epsilon + \mu_2\epsilon^2 + \mu_3\epsilon^3 + \mathcal{O}(\epsilon)^4. \tag{33}$$

For the Schwarzschild with holonomy corrections solution we have

$$\mu_0 = \frac{16\theta_0^4}{16\theta_0^4 - 4(\lambda^2 + 2)^2}, \quad \mu_1 = -\frac{3\pi\theta_0^3(2\lambda^2 + 5)}{2(2\theta_0^2 + \lambda^2 + 2)^3}, \tag{34}$$

$$\begin{aligned}
\mu_2 = &\{3(2\theta_0^2 + \lambda^2 + 2)^5(4\theta_0^2 - 2(\lambda^2 + 2))^2\}^{-1}\Big\{4\theta_0^2\Big[-8D^2(\lambda^2 + 2)^2(2\theta_0^2 + \lambda^2 + 2)^2(-18(\theta_0^2 - 3)\lambda^4 \\
&+ 36(\theta_0^4 - 2\theta_0^2 + 3)\lambda^2 - 8(\theta_0 - 1)(\theta_0 + 1)(\theta_0^4 + 16\theta_0^2 + 1) + 9\lambda^6) - 192D\theta_0^2(\lambda^2 + 2)^3(2\theta_0^2 - \lambda^2 - 2)(2\theta_0^2 + \lambda^2 + 2)^2 \\
&- \frac{1}{2}\theta_0^2(2\theta_0^2 - \lambda^2 - 2)(512\theta_0^4(\lambda^6 + 6\lambda^4 + 18\lambda^2 + 24) + \theta_0^2(512(\lambda^2 + 2)(\lambda^6 + 6\lambda^4 + 18\lambda^2 + 24) - 81\pi^2(2\lambda^2 + 5)^2) \\
&+ 128(\lambda^2 + 2)^2(\lambda^6 + 6\lambda^4 + 18\lambda^2 + 24))\Big]\Big\}. \tag{35}
\end{aligned}$$

We use the expressions for the general case in [73], since $\mathcal{A}_1 \neq 4$. Note that in this case the parameter λ influences already from order zero.

E. Total magnification and centroid

Taking into account (28) and considering that β can also take negative values, we have

$$\theta_0^\pm = \frac{1}{2}\left(\sqrt{\beta^2 + \mathcal{A}_1} \pm |\beta|\right). \tag{36}$$

This means that θ_0^+ is an image that is on the same side as the source and the lens, and θ_0^- is an image that is on the opposite side of both, so that the magnification also becomes $\mu^\pm$. In observations known as microlensing, two or more images cannot be resolved together. What we observe then is the total magnification and the magnification-weighted centroid. As described in [73], these observables have no first order corrections for classical general relativity because $\mathcal{A}_1 = 4$ makes this term zero. For our case this does not occur and we have a nonzero first order term.

Therefore, the total magnification $\mu_t = |\mu^+| + |\mu^-|$, can be rearranged to the following expression

$$\mu_t = -\frac{3\pi\theta_0^3(\theta_0^2 - 1)\lambda^2(2\lambda^2 + 5)(6(\theta_0^2 + 1)^2\lambda^2 + 12(\theta_0^2 + 1)^2 + (\theta_0^4 + \theta_0^2 + 1)\lambda^4)}{2(2\theta_0^2 + \lambda^2 + 2)^3(\theta_0^2(\lambda^2 + 2) + 2)^3}\epsilon + \frac{4(\theta_0^8 - 1)(\lambda^2 + 2)^2}{(4\theta_0^4 - (\lambda^2 + 2)^2)(\theta_0^4(\lambda^2 + 2)^2 - 4)}. \quad (37)$$

We can use the Eq. (28) to give the total magnification as a function of the angle β, but the resulting expression is extremely lengthy, so we do not reproduce it here. In Fig. 4, we show the total magnification highlighting each order $\mu_{t,0}$ and $\mu_{t,1}$ as a function of the angle β. Note that $\mu_{t,1} = 0$ for $\lambda = 0$, which would correspond to the result of classical general relativity. We made $\epsilon = 1$ because we just want to analyze the graphical behavior and of the loop quantum gravity parameter, in observational situations $\epsilon \sim 10^{-4}$.

The magnification-weighted centroid is defined by

$$\Theta = \frac{\theta^+|\mu^+| - \theta^-|\mu^-|}{|\mu^+| + |\mu^-|}, \quad (38)$$

which leads to

$$\Theta = \frac{4(\theta_0^8 - \theta_0^6 + \theta_0^4 - \theta_0^2 + 1)(\lambda^2 + 2)^2 - 16\theta_0^4}{4\theta_0(\theta_0^6 - \theta_0^4 + \theta_0^2 - 1)(\lambda^2 + 2)^2} + \epsilon\left\{3\pi\theta_0^2\lambda^2(2\lambda^2 + 5)\right.$$
$$\times \left[\frac{1}{4}(\theta_0^{12} + 1)(\lambda^2 + 2)^2(9\pi^2(2\lambda^2 + 5)^2 + 128(\lambda^2 + 4)) + 16\theta_0^6(\lambda^8 + 20\lambda^6 + 104\lambda^4 + 208\lambda^2 + 160)\right.$$
$$\left.+ 16(\theta_0^4 + 1)\theta_0^4(\lambda^8 + 12\lambda^6 + 40\lambda^4 + 40\lambda^2 + 16) + 32(\theta_0^8 + 1)\theta_0^2(\lambda^2 + 2)(\lambda^4 + 4\lambda^2 - 4)\right]\right\}$$
$$\times \left\{128(\theta_0^4 - 1)(\theta_0^4 + 1)^2(\lambda^2 + 2)^4(2\theta_0^2 + \lambda^2 + 2)(\theta_0^2(\lambda^2 + 2) + 2)\right\}^{-1}. \quad (39)$$

The expression of this observable as a function of the angle β is also too extensive and we have therefore decided not to write it here. However, we show in the Fig. 5 the magnification-weighted centroid as a function of this angle for different values of λ. We note that, again, the first-order component is zero when $\lambda = 0$.

F. Time delay

The path followed by the photons of the first image with positive parity and the second image with negative parity is different and with this we can calculate the associated delay time. We can write the delay time and the first-order correction in the form [80]

$$\Delta\tau = \Delta\tau_0 + \Delta\tau_1\epsilon + \mathcal{O}(\epsilon)^2, \quad (40)$$

where

$$\Delta\tau_0 = \frac{1}{2}|\beta|\sqrt{\mathcal{A}_1 + \beta^2} + \frac{\mathcal{A}_1}{4}\ln\left(\frac{\sqrt{\mathcal{A}_1 + \beta^2} + \beta}{\sqrt{\mathcal{A}_1 + \beta^2} - \beta}\right),$$

$$\Delta\tau_1 = \frac{\mathcal{A}_2}{\mathcal{A}_1}|\beta|. \quad (41)$$

From Eq. (41) it is clear that at $\beta = 0$ (source, lens, and observer are aligned) we have the Einstein ring and there is
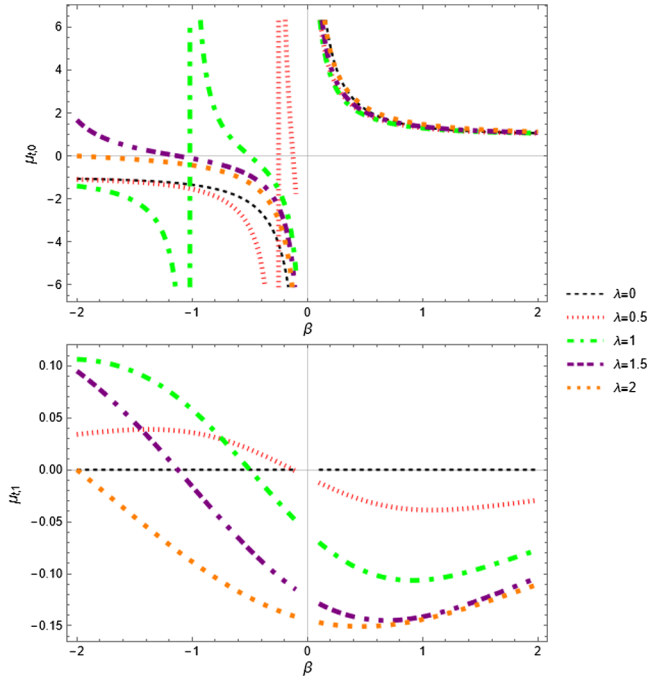

FIG. 4. Graphical representation of the total magnification, given by the Eq. (37), as a function of the angle β. We considered $\epsilon = 1$. We have the positive-parity image when $\beta > 0$ and negative-parity image for $\beta < 0$. We omit the regions with $|\beta| = 0.1$ for obvious physical reasons.
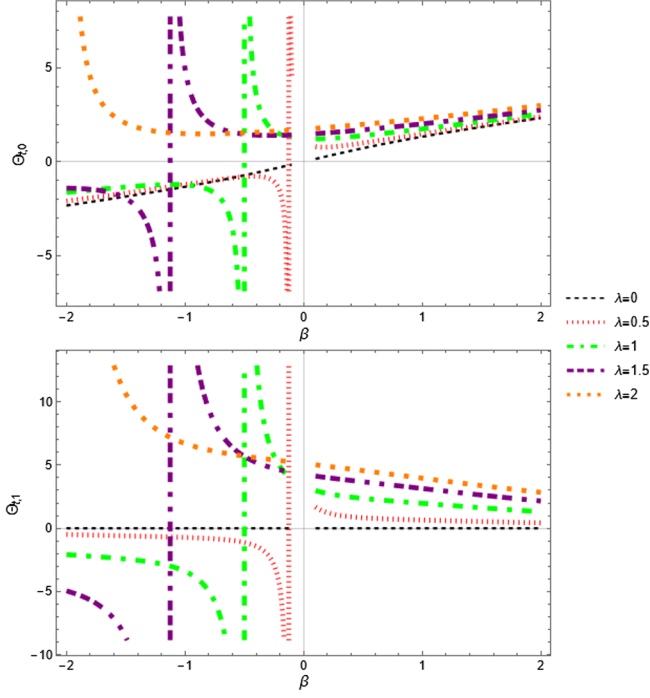
FIG. 5. Graphical representation of the magnification-weighted centroid, given by the Eq. (39), as a function of the angle β, where we consider $\epsilon = 1$. We have the positive-parity image when $\beta > 0$ and negative-parity image for $\beta < 0$. We omit the regions with $|\beta| = 0.01$ for obvious physical reasons.

no delay between images. If we now consider the coefficients given by Eq. (23), we get that

$$\Delta\tau_0 = \frac{1}{2}\beta\sqrt{\beta^2 + 2(\lambda^2 + 2)}$$
$$+ \frac{1}{2}(\lambda^2 + 2)\ln\left(\frac{\sqrt{\beta^2 + 2(\lambda^2 + 2)} + \beta}{\sqrt{\beta^2 + 2(\lambda^2 + 2)} - \beta}\right),$$

$$\Delta\tau_1 = \frac{3\pi\beta(2\lambda^2 + 5)}{8(\lambda^2 + 2)}, \tag{42}$$

this means that the lambda parameter increases the delay time. In Fig. 6 we show the influence of β on the coefficients $\Delta\tau_{0,1}$ for different values of λ.

III. DEFLECTION ANGLE BY GAUSS-BONNET THEOREM

In this section we will re-derive the coefficient $\mathcal{A}_1$ for the deflection angle in the weak field regime using the method described in [81]. Its equivalence with the geodesic method was shown in [82]. In summary, Gibbons and Werner proposed that the Gauss-Bonnet theorem can be used to calculate the deflection angle in the form

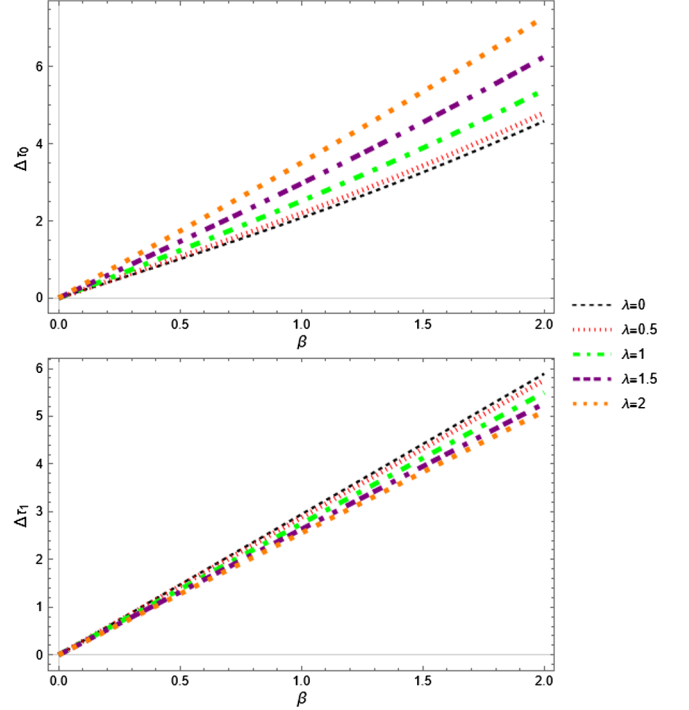$$\alpha = -\int_0^\pi \int_{r_{sl}}^\infty K dS. \tag{43}$$

FIG. 6. Graphical representation of the time delay coefficients, given by the Eq. (42), as a function of the angle β.

Here K is the optical Gaussian curvature and r_{sl} is the distance traveled by the photon considering the approximation of a straight line path. We consider, without loss of generality, that the movement takes place in the equatorial plane where $\theta = \pi/2$, so we have

$$ds^2 = -A(r)dt^2 + B(r)dr^2 + C(r)d\phi^2. \tag{44}$$

From that metric we derive the optical metric $\bar{g}_{ij}$ from the relation

$$dt^2 = \bar{g}_{rr}dr^2 + \bar{g}_{\phi\phi}d\phi^2 = \frac{B(r)}{A(r)}dr^2 + \frac{C(r)}{A(r)}d\phi^2. \tag{45}$$

We assume that the geodesics of photons obey $ds^2 = 0$. The Gaussian curvature K is defined in terms of the new metric $\bar{g}_{ij}$ as follows

$$K = -\frac{1}{\sqrt{\bar{g}_{rr}\bar{g}_{\phi\phi}}}\left[\frac{\partial}{\partial r}\left(\frac{1}{\sqrt{\bar{g}_{rr}}}\frac{\partial\sqrt{\bar{g}_{\phi\phi}}}{\partial r}\right) + \frac{\partial}{\partial\phi}\left(\frac{1}{\sqrt{\bar{g}_{\phi\phi}}}\frac{\partial\sqrt{\bar{g}_{rr}}}{\partial\phi}\right)\right]. \tag{46}$$

In addition, we have that

$$dS^2 = \sqrt{\det|\bar{g}|}drd\phi, \tag{47}$$

and

$$r_{sl} = \frac{u}{\sin\phi}. \tag{48}$$

Let us now apply this formalism and calculate the first coefficient of the deflection angle expansion in the weak field regime. From the Eq. (18) we have

$$\bar{g}_{rr} = \frac{1}{(1 - \frac{2m}{r})^2(1 - \frac{2m\lambda^2}{(\lambda^2+1)r})}, \qquad \bar{g}_{\phi\phi} = \frac{r^2}{1 - \frac{2m}{r}}. \tag{49}$$

Substituting Eq. (49) into Eq. (46) and considering a Taylor series expansion up to the order of λ^2 we get

$$\alpha = -\int_0^\pi \int_{\frac{u}{\sin\phi}}^\infty \left[\frac{m(3m - 2r)}{(r - 2m)^3(\frac{r}{r-2M})^{3/2}} \right. \\ \left. + \frac{\lambda^2 m(9m^2 - 7mr + r^2)(-\frac{r}{2M-r})^{3/2}}{r^4} + \mathcal{O}(\lambda^4) \right] dr d\phi. \tag{50}$$

The first integral, in the coordinate r, results in

$$\alpha = -\int_0^\pi \left[1 - \frac{\lambda^2 m \sin(\phi)(u - 3m\sin(\phi))\sqrt{\frac{u}{u-2m\sin(\phi)}}}{u^2} \right. \\ \left. + \frac{3m\sqrt{\frac{1}{1-2\sin(\phi)}}\sin(\phi)}{u} - \sqrt{\frac{u}{u - 2m\sin(\phi)}} \right] d\phi. \tag{51}$$

As we are dealing with the weak field regime, where $m/u \ll 1$, we rewrite the above integral considering a Taylor series expansion as follows

$$\alpha = -\int_0^\pi \left[-\frac{3m\sin(\phi)(\frac{m\sin(\phi)}{u} + 1)}{u} - \frac{\lambda^2 m \sin(\phi)}{u} \right. \\ \left. + \frac{m\sin(\phi)}{u} + \mathcal{O}\left(\frac{m}{u}\right)^2 \right] d\phi. \tag{52}$$

The result is then

$$\alpha = 2(2 + \lambda^2)\frac{m}{u}. \tag{53}$$

Therefore, we recover the same $\mathcal{A}_1$ found by the geodesics method (23) in Sec. II.

IV. STRONG GRAVITATIONAL LENSING

In the previous section, we used a formalism that applies to the case where the closest approach (r_0) distance is much larger compared to the mass of the lens (in our case, the black hole). In this section, we will discuss the deflection of light in the so-called strong field regime. From the point of view of the classical mechanics we would expect that the light (or the particles) can approach

the event horizon freely and would be in an "inaccessible" region only after crossing it. But this is not what actually happens. In fact, the light is absorbed by the black hole when it is sent with a radius smaller than the critical impact parameter (u_m) of the solution. K. Virbhadra and G. Ellis [46] studied the gravitational lensing effect for the Schwarzschild solution and showed that it occurs for the value $r_0 < 3\sqrt{3}m$. They also showed that $r = 3m$ delimits a surface on which any null geodesic starting at any point on the surface and initially tangent to it remains in the same surface, which we call the photon sphere. In any spacetime containing a photonsphere, gravitational lensing leads to relativistic images [46]. As $r_0 \to r_m$ (or $u \to u_m$), the deflection angle increases and consequently diverges to $r_0 = r_m$ (or $u = u_m$). This concept of the photon surface of the Schwarzschild solution was generalized in [47], we can calculate r_m by

$$\frac{C'(r)}{C(r)} = \frac{A'(r)}{A(r)}. \tag{54}$$

So, in this section we study the deflection of light in the limit where the geodesics pass close to the photon surface.

A. Deflection angle

Considering that the deflection angle tends to infinity as $r_0 \to r_m$, Bozza [58] proposed that in this limit α can be approximated by a logarithmic expansion of the form

$$\alpha(u) = b_1 \log\left(\frac{u}{u_m} - 1\right) + b_2 + \mathcal{O}(u - u_m), \tag{55}$$

where b_1, b_2 and u_m are coefficients to be calculated from the metric. The critical impact parameter u_m is obtained directly from Eq. (11) if we equate the distance of closest approach x_0 with the radius of the photon sphere x_m. We will briefly discuss how to obtain the other two coefficients. We emphasize that the starting point is the same as before, namely to propose an approximate result for the integral (6). First, we assume the metric (we use the substitution $x = r/2m$)

$$ds^2 = -A(x)dt^2 + B(x)dr^2 + C(x)d\Omega^2, \tag{56}$$

Then, we define the variables

$$y = A(x), \tag{57}$$

$$\zeta = \frac{y - y_0}{1 - y_0}, \tag{58}$$

where $y_0 = A(x_0)$. This leads to

$$\alpha(x_0) = I(x_0) - \pi, \tag{59}$$

$$I(x_0) = \int_0^1 R(\zeta, x_0) f(\zeta, x_0) d\zeta. \tag{60}$$

Here the function $R(\zeta, x_0)$ is given by

$$R(\zeta, x_0) = \frac{2\sqrt{By}}{CA'}(1 - y_0)C_0, \tag{61}$$

which is regular for any value of ζ and x_0. The function $f(\zeta, x_0)$ is provided by

$$f(\zeta, x_0) = \frac{1}{\sqrt{y_0 - [(1 - y_0)\zeta + y_0]\frac{C_0}{C}}}, \tag{62}$$

which has a divergence for $\zeta \to 0$. All functions without the subscript 0 are evaluated at $x = A^{-1}[(1 - y_0)\zeta + y_0]$. We rewrite $f(\zeta, x_0)$ as

$$f(\zeta, x_0) \sim f_0(\zeta, x_0) = \frac{1}{\sqrt{\beta_1\zeta + \beta_2\zeta^2}}, \tag{63}$$

where

$$\beta_1 = \frac{1 - y_0}{C_0 A_0'}(C_0'y_0 - C_0 A_0'), \tag{64}$$

and

$$\beta_2 = \frac{(1 - y_0)^2}{2C_0^2 A_0'^3}[2C_0 C_0' A_0'^2 + (C_0 C_0'' - 2C_0'^2)y_0 A_0'$$
$$- C_0 C_0' y_0 A_0'']. \tag{65}$$

In the form (63) we can see that: If $\beta_1 \neq 0$, the leading order of divergence in (62) is $\zeta^{-1/2}$, and if $\beta_1 = 0$ the divergence is ζ^{-1}. In the first case f_0 can be integrated and the result is finite, while in the second case the integral diverges. Returning to the original variables, we note that β_1 vanishes at $x_0 = x_m$, and in order to solve this problem, we treat the integral (60) as follows

$$I(x_0) = I_D(x_0) + I_R(x_0), \tag{66}$$

where

$$I_D(x_0) = \int_0^1 R(0, x_m) f_0(\zeta, x_0) d\zeta, \tag{67}$$

refers to the divergent part, and

$$I_R(x_0) = \int_0^1 g(\zeta, x_0) d\zeta, \tag{68}$$

with

$$g(\zeta, x_0) = R(\zeta, x_0) f(\zeta, x_0) - R(0, x_m) f_0(\zeta, x_0). \tag{69}$$

Note that $I_R = I - I_D$. The result of these integrals is [58]

$$I_D(x_0) = -\left(\frac{R(0, x_m)}{\sqrt{\beta_{2m}}}\right) \log\left(\frac{x_0}{x_m} - 1\right)$$
$$+ \frac{R(0, x_m)}{\sqrt{\beta_{2m}}} \log \frac{2(1 - y_m)}{A_m' x_m} + \mathcal{O}(x_0 - x_m), \tag{70}$$

and

$$I_R(x_m) = \int_0^1 g(\zeta, x_m) d\zeta + \mathcal{O}(x_0 - x_m). \tag{71}$$

Functions with index m are calculated in $x_0 = x_m$. The logarithmic approximation for the deflection angle is then

$$\alpha(x_0) = -\left(\frac{R(0, x_m)}{\sqrt{\beta_{2m}}}\right) \log\left(\frac{x_0}{x_m} - 1\right)$$
$$+ \frac{R(0, x_m)}{\sqrt{\beta_{2m}}} \log \frac{2(1 - y_m)}{A_m' x_m}$$
$$+ \int_0^1 g(\zeta, x_m) d\zeta - \pi + \mathcal{O}(x_0 - x_m). \tag{72}$$

As stated in the previous section, it is convenient to write this result in terms of the gauge invariant coordinate u. We can expand Eq. (11) and write

$$u - u_m = \beta_{2m}\sqrt{\frac{y_m}{C_m^3}\frac{C_m'^2}{2(1 - y_m^2)}}(x_0 - x_m)^2. \tag{73}$$

With the above equation we can write Eq. (72) in the form (55), where the coefficients b_1 and b_2 are

$$b_1 = \frac{R(0, x_m)}{2\sqrt{\beta_{2m}}}, \tag{74}$$

$$b_2 = \int_0^1 g(\zeta, x_m) d\zeta + b_1 \log \frac{2\beta_{2m}}{y_m} - \pi. \tag{75}$$

Let us now apply this mechanism to the Schwarzschild solution. In standard coordinates, the metric is

$$A(x) = 1 - \frac{1}{x},$$
$$B(x) = A(x)^{-1},$$
$$C(x) = x^2. \tag{76}$$

The first step is to find the radius of the photon sphere x_m from Eq. (54), which in this case is
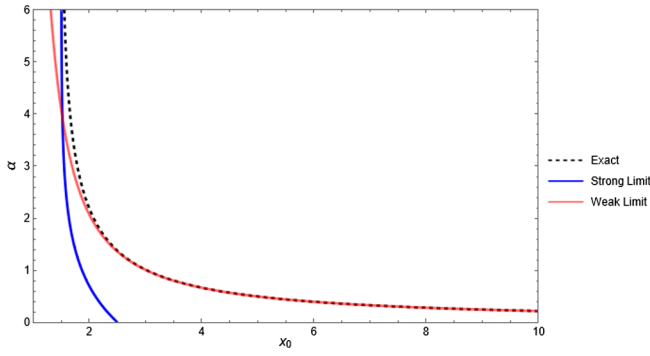
$$x_m = \frac{3}{2}, \tag{77}$$

FIG. 7. Graphical representation of the deflection angle for the Schwarzschild solution.

Substituting this result into Eq. (11), we immediately get $u_m = 3\sqrt{3}/2$. The functions $R(\zeta, x_0)$ and $f(\zeta, x_0)$ are given by

$$R(\zeta, x_0) = 2,$$

$$f(\zeta, x_0) = \frac{1}{\sqrt{\beta_1 \zeta + \beta_2 \zeta^2 - \frac{\zeta^3}{x_0}}}, \tag{78}$$

respectively, where, from Eqs. (64) and (65), we have

$$\beta_1 = 2 - \frac{3}{x_m} = 0,$$

$$\beta_2 = \frac{3}{x_m} - 1 = 1. \tag{79}$$

and with these results we find $b_1 = 1$. The integral I_R is

$$I_R(x_m) = \int_0^1 g(\zeta, x_m) d\zeta = 0.9496, \tag{80}$$

then $b_2 = -0.4002$. Putting these results together, we get the logarithmic expansion for the deflection angle as a function of the impact parameter, given by

$$\alpha(u) = \log\left(\frac{2u}{3\sqrt{3}} - 1\right) - 0.4002. \tag{81}$$

In Fig. 7 we show the exact deflection angle [computed numerically with the integral (6)] and the strong/weak field approximations. We see that both the logarithmic expansion (blue line) and the exact values (dotted line) diverge at $x_0 \to x_m = 1.5$, but these curves move away rapidly as x_0 increases. In contrast, the weak-field expansion approaches the exact result as x_0 increases.

For the Schwarzschild solution with holonomy corrections we consider the following metric

$$A(x) = 1 - \frac{1}{x},$$

$$B(x) = \frac{1}{(1 - \frac{1}{x})(1 - \frac{\lambda^2}{(\lambda^2 + 1)x})},$$

$$C(x) = x^2. \tag{82}$$

$$x_m = \frac{3}{2} \tag{83}$$

$$u_m = \frac{3\sqrt{3}}{2} \tag{84}$$

$$R(\zeta, x_0) = 2\sqrt{\frac{\lambda^2 + 1}{\frac{\lambda^2}{3} + 1}},$$

$$f(\zeta, x_0) = \frac{1}{\sqrt{\beta_1 \zeta + \beta_2 \zeta^2 - \frac{\zeta^3}{x_0}}}, \tag{85}$$

with the same $\beta_{1,2}$ from Eq. (79). This leads to

$$b_1 = \frac{R(0, x_m)}{2\sqrt{\beta_{2m}}} = \sqrt{\frac{\lambda^2 + 1}{\frac{\lambda^2}{3} + 1}}. \tag{86}$$

To compute b_2 we first write the function

$$g(\zeta, x_m) = \frac{2}{z}\left(\frac{3z\sqrt{\frac{\lambda^2 + 1}{\lambda^2 + 2\lambda^2 z + 3}}}{\sqrt{z^2(3 - 2z)}} - \sqrt{3}\sqrt{\frac{\lambda^2 + 1}{\lambda^2 + 3}}\right), \tag{87}$$

which if integrated results in

$$\int g(\zeta, x_m) d\zeta = -2\sqrt{3}\left(\sqrt{\frac{\lambda^2 + 1}{\lambda^2 + 3}}\ln(z) + \frac{2\sqrt{\frac{\lambda^2 + 1}{\lambda^2 + 2\lambda^2 z + 3}}\sqrt{\lambda^2(2z + 1) + 3}\tan^{-1}\left(\frac{\sqrt{\lambda^2 + 3}\sqrt{3 - 2z}}{\sqrt{\lambda^2(6z + 3) + 9}}\right)}{\sqrt{\lambda^2 + 3}}\right) + C. \tag{88}$$

It is easy to see that the Schwarzschild result is immediately recovered if we use $\lambda = 0$. The presence of the constant λ in the above equation makes it impossible to determine the limit in $z = 0$ analytically. Because of this limitation, we solve this integral numerically with values of the constant from zero to two. From this we can calculate the coefficient b_2, and show the result of the coefficients of the expansion of the deflection angle in Fig. 8. In the Figs. 9–11 we show respectively the deflection angle as a function of the constant λ, the impact parameter u and the reduced impact parameter u/u_m.
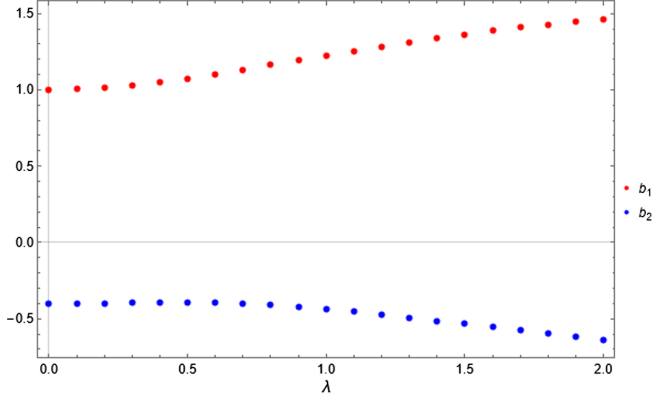
FIG. 8. Graphical representation, for the Schwarzschild solution with holonomy corrections, of the coefficients as a function of the parameter λ.
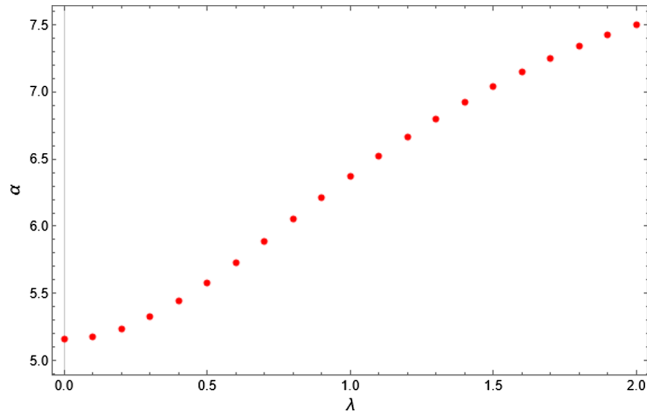

FIG. 9. Graphical representation, for the Schwarzschild solution with holonomy corrections, of the deflection angle as a function of the parameter λ.
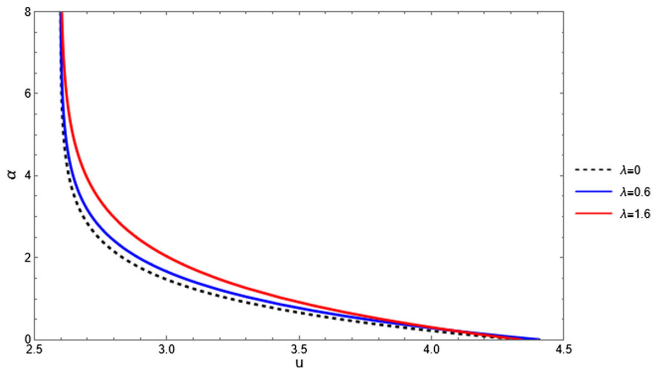

FIG. 10. Graphical representation, for the Schwarzschild solution with holonomy corrections, of the deflection angle as a function of the impact parameter.
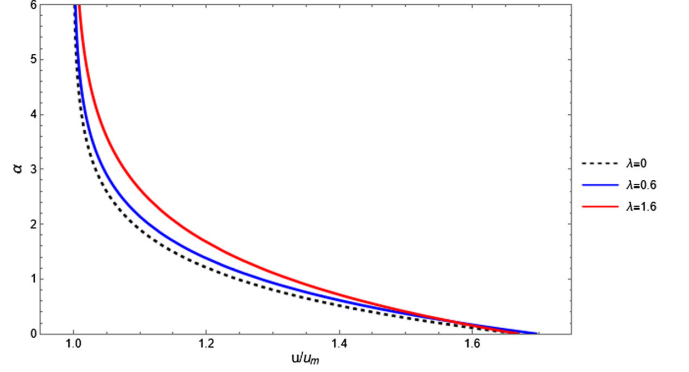

FIG. 11. Graphical representation, for the Schwarzschild solution with holonomy corrections, of the deflection angle as a function of the reduced impact parameter.

V. OBSERVABLES FOR THE SAGITTARIUS A*

In this section we analyze the influence of the λ parameter on the observables for both the weak and strong field regimes. We consider the mass and distance with respect to the black hole at the center of our galaxy, Sagittarius A*, which (we ignore uncertainties) is [83–85]

$$m = 4.297 \times 10^6 M_\odot,$$
$$D_{OL} = 2.55402 \times 10^{20} \qquad (89)$$

where $M_\odot = 1.98892 \times 10^{30}$ kg is the Solar mass. Recall that we use geometric units unless otherwise noted. As suggested in Sec. II, the observables are the positions of the lensed images, the magnification, and the delay time between them. But before we turn to the numerical example, we need to clarify two points. First, we will work with flux rather than magnification (following [58,74]). In addition, we will consider different situations for each regime. For the weak field, we consider two lensed images, the first with positive parity and the second with negative parity. In the strong field, the photon can make loops around the black hole before emerge into infinity and reach the observer. Therefore, we will consider observables that relate the first image and the contribution of all others.

A. Weak field

For this regime we will consider a combination of the observables we worked on in Sec. II, they are

$$P_t = \vartheta^+ + \vartheta^- = \sqrt{A_1\theta_E{}^2 + \beta^2} + \frac{\epsilon A_2 \theta_E}{A_1}, \qquad (90)$$

$$\Delta P = \vartheta^+ - \vartheta^- = |\beta| - \frac{|\beta|\theta_E}{\sqrt{A_1\theta_E{}^2 + \beta^2}}\epsilon, \qquad (91)$$

$$F_t = F^+ + F^- = \frac{F_{\text{src}}(A_1\theta_E{}^2 + 2\beta^2)}{2|\beta|\sqrt{A_1\theta_E{}^2 + \beta^2}}, \qquad (92)$$

$$\Delta F = F^+ - F^- = F_{\text{src}} - \frac{A_2 F_{\text{src}} \theta_E{}^3}{2(A_1 \theta_E{}^2 + \beta^2)^{3/2}} \epsilon \tag{93}$$

$$\Theta_{\text{cent}} = \frac{\vartheta^+ F^+ - \vartheta^- F^-}{F_t} = \frac{|\beta|(3A_1 \theta_E{}^2 + 4\beta^2)}{2A_1 \theta_E{}^2 + 4\beta^2} \tag{94}$$

$$\Delta\tau = \frac{D_{OL} D_{OS} \left(\frac{1}{2}|\beta|\sqrt{A_1\theta_E{}^2 + \beta^2} + \frac{1}{4}A_1\theta_E{}^2 \ln\left(\frac{\sqrt{A_1\theta_E{}^2+\beta^2}+|\beta|}{\sqrt{A_1\theta_E{}^2+\beta^2}-|\beta|} \right) + \frac{|\beta|A_2\theta_E}{A_1}\epsilon \right)}{cD_{LS}}. \tag{95}$$

The flux is related to magnification by $F_i = |\mu_i| F_{\text{src}}$, where F_{src} is the source flux. To calculate this numerically, we use the Eqs. (24) and (25). First, however, we need to convert the values in (89) to more appropriate units, i.e., parsecs (pc). We will use the following values

$$m = 4.297 \times 10^6 M_\odot = 2.057 \times 10^{-7} \text{ pc},$$
$$D_{OL} = 2.55402 \times 10^{20} = 8.277 \text{ kpc} \tag{96}$$

this choice of units leads to $\vartheta_E = 0.0225813\sqrt{d_{ls}}$ and $\epsilon = 0.000181799/\sqrt{d_{ls}}$. we assume that $d_{ls} = D_{LS}/1(pc)$ to simplify notation. This distance is usually much smaller than the distance from the observer to the source D_{OS} and from the observer to the lens D_{OL}. In other words, $D_{OL} \sim D_{OS} \gg D_{LS}$. The following figures show the behavior of the practical observables as a function of the source angle β and the loop quantum gravity parameter λ, we have $d_{ls} = 1$ in all cases. We can see that the influence of λ on

the values of the observables in the considered intervals is practically zero. Figure 12 shows the angular distance P_t and Fig. 13 shows the difference of the angular positions ΔP, both increase with β. The total flux F_t, shown in Fig. 14, and the flux difference ΔF, shown in Fig. 15, are constant for $\beta 2$; below this value we see that F_t increases while ΔF decreases. However, these fluctuations are small. Figure 16 shows the centroid Θ_{cent} and Fig. 17 shows the differential time delay $\Delta\tau$, both observables also increase with angle β.

B. Strong field

Here we focus on the asymptotic position approached by a set of images ϑ_∞, the distance between the first image (labeled ϑ_1) and the others s, the ratio between the flux of the first image and the flux of all the other images r_m [58], and in the time delay between one photon with 2 loops from on photon with one loop around the lens [72]. These are given by
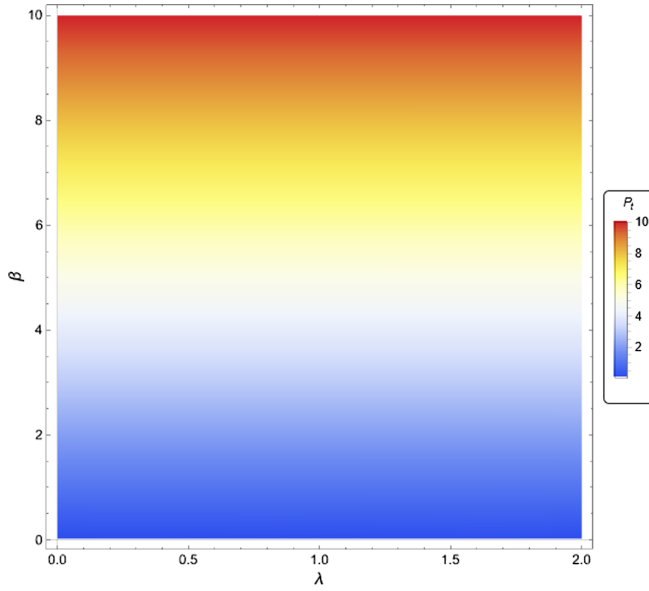

FIG. 12. Density plot, for the Schwarzschild solution with holonomy corrections, of the angular distance between two lensed images P_t (m arc s), given by the equation (90), as a function of the angle β and the parameter λ.
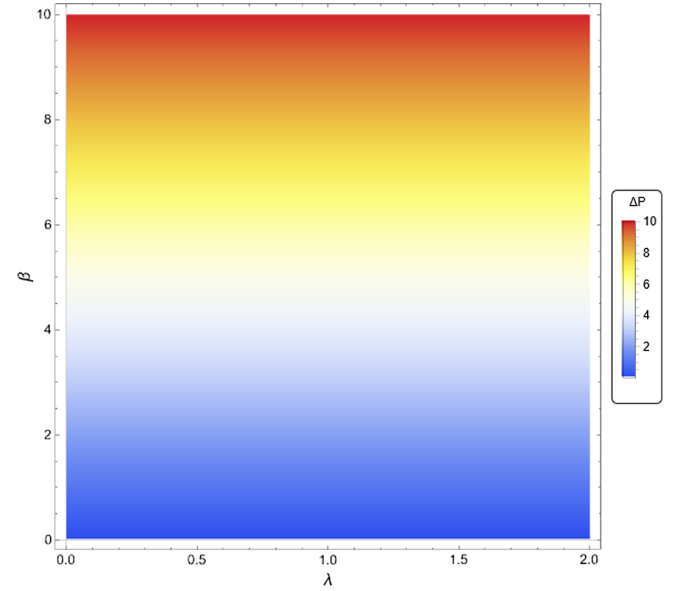

FIG. 13. Density plot, for the Schwarzschild solution with holonomy corrections, of the difference of the angular positions between two lensed images ΔP (m arc s), given by the equation (91), as function of the angle β and the parameter λ.
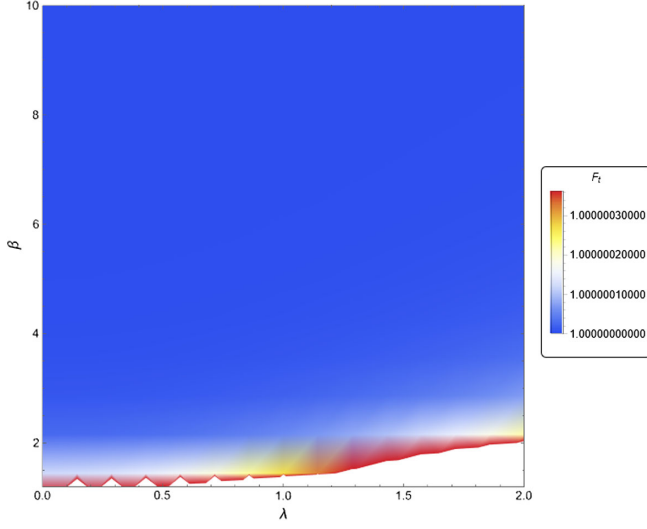
FIG. 14. Density plot, for the Schwarzschild solution with holonomy corrections, of the total flux between two lensed images F_t, given by the Eq. (92), as function of the angle β and the parameter λ.

$$\vartheta_\infty = \frac{u_m}{D_{OL}}, \tag{97}$$

$$s = \vartheta_1 - \vartheta_\infty = \vartheta_\infty e^{\frac{b_2 - 2\pi}{b_1}}, \tag{98}$$

$$r_m = e^{\frac{2\pi}{b_1}}, \tag{99}$$

$$\Delta T_{2,1} = [2\pi - 2\gamma]u_m + 2\sqrt{\frac{B_m}{A_m}}\sqrt{\frac{u_m}{c_1}}e^{\frac{b_2}{2b_1}}\left(e^{-\frac{\pi\gamma}{b_1}} - e^{-\frac{2\pi\gamma}{b_1}}\right). \tag{100}$$
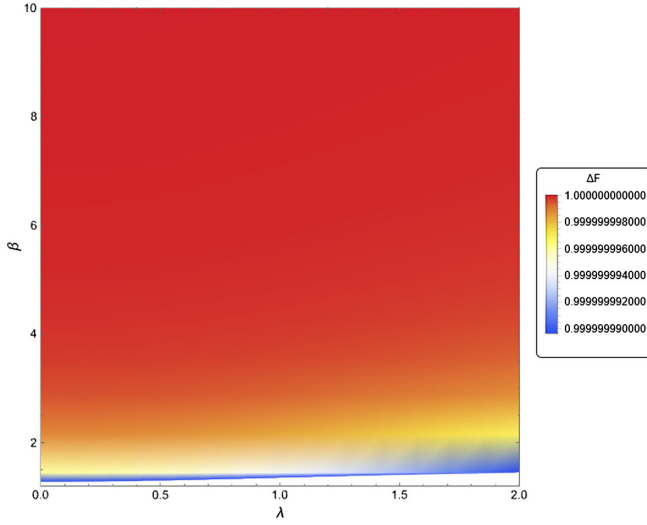

FIG. 15. Density plot, for the Schwarzschild solution with holonomy corrections, of the difference of flux between two lensed images ΔF, given by the equation (93), as function of the angle β and the parameter λ.
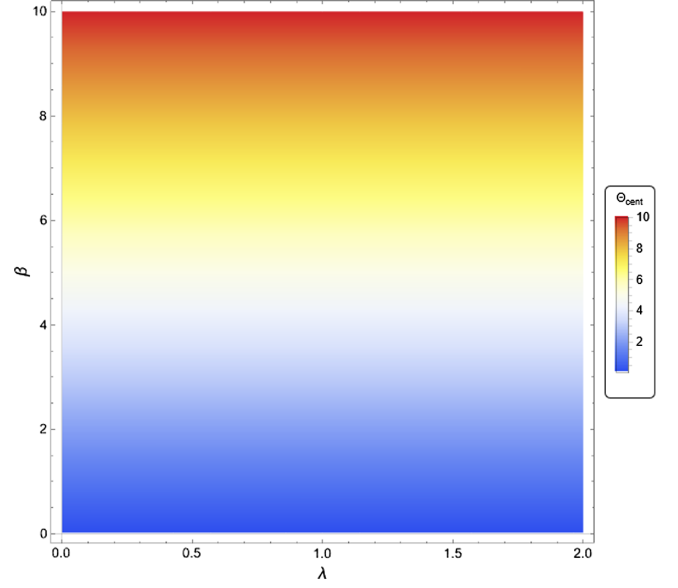

FIG. 16. Density plot, for the Schwarzschild solution with holonomy corrections, of the differential time delay between two lensed images Θ_{cent} (m arc s), given by the Eq. (94), as function of the angle β and the parameter λ.

In the time expression, γ stands for the angular distance between the source and the optical axis as seen from the lens. In real observations, this angle should be of the order $\gamma \sim D_{OL}^{-1}$. With the values in (89), we obtain the data listed in Table I. Since ϑ_∞ does not depend on λ, the result is 26.5807 μarcsecs (the same as in the Schwarzschild case) and we therefore do not include it in the table. We note that the distance between the first and the other images increases
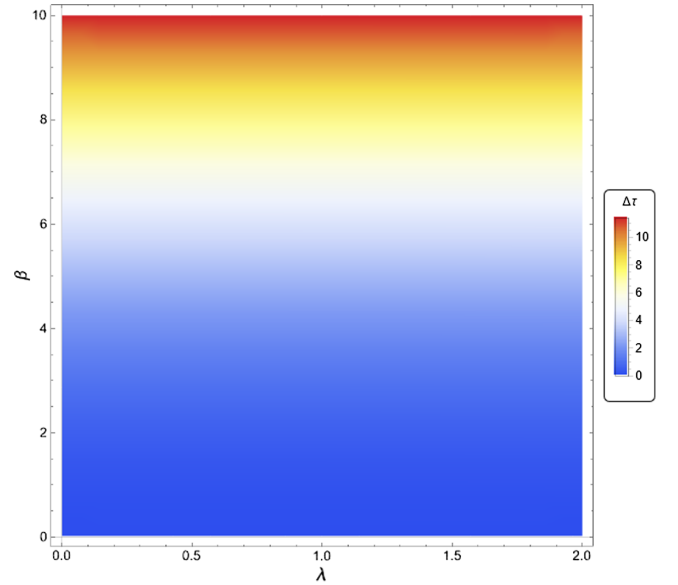

FIG. 17. Density plot, for the Schwarzschild solution with holonomy corrections, of $\Delta\tau$ (s), given by the Eq. (95), as function of the angle β and the parameter λ.

TABLE I. Estimates for the main observables and the strong field limit coefficients for the black hole in the center of our galaxy considering the Schwarzschild geometry with holomy corrections.

λ	b_1	b_2	s (μarcsecs)	r_m	$\Delta T_{2,1}$ (hours)
0	1	−0.40023	0.0332657	6.82188	0.19431
0.1	1.00332	−0.399568	0.0340313	6.79933	0.194315
0.2	1.01307	−0.397839	0.0363476	6.73385	0.19433
0.3	1.02871	−0.395748	0.0402631	6.63147	0.194354
0.4	1.04941	−0.394252	0.0458289	6.50067	0.194385
0.5	1.07417	−0.394335	0.0530645	6.35083	0.194423
0.6	1.10195	−0.396812	0.0619262	6.19076	0.194466
0.7	1.13173	−0.402209	0.0722898	6.02786	0.194512
0.8	1.1626	−0.410737	0.083952	5.86776	0.194559
0.9	1.19382	−0.422324	0.0966477	5.71435	0.194607
1	1.22474	−0.436684	0.110078	5.57004	0.194654
1.1	1.25492	−0.453397	0.12394	5.43611	0.1947
1.2	1.284	−0.471976	0.137951	5.313	0.194745
1.3	1.31175	−0.491927	0.151865	5.2006	0.194787
1.4	1.33803	−0.512787	0.16548	5.09845	0.194828
1.5	1.36277	−0.534139	0.178644	5.00589	0.194866
1.6	1.38595	−0.555633	0.191246	4.92216	0.194901
1.7	1.4076	−0.576979	0.203215	4.84648	0.194934
1.8	1.42775	−0.59795	0.214512	4.77807	0.194965
1.9	1.44647	−0.618373	0.225122	4.71622	0.194994
2	1.46385	−0.638122	0.235048	4.66023	0.195021

with λ, and so does the delay time between them. The decrease in r_m means that the first image becomes less intense compared to the other images as the parameter λ increases. In addition, it is clear that the delay time for this regime is more intense when compared to the weak field regime.

VI. MASSIVE PARTICLES SURFACE

The photon surface concept used in Sec. IV also plays an important role in the study of black hole shadows. We will not deal with shadows here, but we would like to introduce a generalization of this concept, namely the surface of massive particles. In [86] the authors propose a generalization of the photon surface for the case of massive and charged particles. They define a surface which also has the main property of a photon sphere, i.e.: any world line originally tangent to the surface of a massive particle remains tangent to it. The main difference between these two definitions is that the photon sphere formalism considers null geodesics with a fixed impact parameter, while for massive particles the fixed parameter is the total energy. A full description of this approach and its main implications can be found in [86]. Here we restrict ourselves to the calculation of the surface for a neutral particle of mass m_0 in a spacetime described by the holonomy-corrected Schwarzschild solution. We start considering the static metric tensor

$$ds^2 = -Adt^2 + Bdr^2 + Cd\phi^2 + Dd\theta^2 \quad (101)$$

where A, B, C and D are free functions of r and θ, but we choose a surface with $r =$ const. The main equation of this method (for neutral particles) is

$$\varepsilon_\pm = \pm m_o \sqrt{\frac{\kappa^2 \chi_\tau}{K}}. \quad (102)$$

Here ε is the total energy. According to [86], $d\varepsilon/dr = 0$ defines marginally stable orbits, such as the innermost stable circular orbit (ISCO). And the value of r at which the energy diverges defines the photon surface. In order to calculate the total energy (102), we must first calculate the second fundamental form and its trace, which (for this particular static spacetime) is defined as follows

$$\chi_{\mu\nu} = \frac{1}{2\sqrt{B}}(-\partial_r Adt^2 + \partial_r Cd\phi + \partial_r Dd\theta), \quad (103)$$

$$\chi = \chi^\mu{}_\nu = \frac{\partial_r \ln(ADC)}{2\sqrt{B}}. \quad (104)$$

Also, we have that the killing vector is $\kappa^\mu \partial_\mu = \partial_t$ and then $\kappa^\mu \kappa_\mu = -A$. And finally, we have

$$K = 3\chi_\tau - 2\chi, \quad (105)$$

where χ_τ for this static space time is

$$\chi_\tau = \frac{2\sqrt{A}}{r}. \quad (106)$$

If we consider the Schwarzschild metric (8), for example, we have

$$\chi_\tau = \frac{2}{r}\sqrt{1 - \frac{2m}{r}}, \qquad \chi = \left(\frac{1}{\sqrt{1 - \frac{2m}{r}}}\right)\frac{2r - 3m}{r^2},$$

$$\kappa^2 = -1 + \frac{2m}{r}, \qquad K = 2\left(\frac{1}{\sqrt{1 - \frac{2m}{r}}}\right)\frac{3m - r}{r^2}. \quad (107)$$

So, the total energy for this case is

$$\varepsilon^2/m_0^2 = \frac{(r - 2m)^2}{r(r - 3m)}. \quad (108)$$

It is easy to see that the above expression diverges for $r = 3m$, so we get the well-known result for the radius of the photon sphere. If we equate $d\varepsilon/dr = 0$, we get $r = 6m$, which represents the ISCO.

If we now proceed to the holonomy-corrected solution, we consider the metric (18) and then have

$$\chi = \frac{(2r-3m)\sqrt{\frac{\lambda^2(r-2m)+r}{(\lambda^2+1)(r-2m)}}}{r^2},$$

$$K = \frac{2\left((2r-3m)\sqrt{1-\frac{2m}{(\lambda^2+1)(2m-r)}}-3r\sqrt{1-\frac{2m}{r}}\right)}{r^2}. \quad (109)$$

The quantities χ_τ and κ^2 are the same as (107). With these values, the energy is

$$\epsilon^2/m_0^2 = -\frac{r(1-\frac{2m}{r})^{3/2}}{(2r-3m)\sqrt{1-\frac{2m}{(\lambda^2+1)(2m-r)}}-3r\sqrt{1-\frac{2m}{r}}}. \quad (110)$$

We can simplify this expression by making the following change to the variable $R = r/m$. This leads us to

$$\epsilon^2/m_0^2 = \frac{2-R}{R\left(\frac{\sqrt{\frac{1}{\lambda^2+1}}(2R-3)}{R-2}-3\right)}. \quad (111)$$

Now, by taking the derivative of the above equation, we can find the radius of the massive particle surface. This operation results in

$$r_{\text{ISCO}} = \frac{6m\left(\sqrt{\frac{1}{\lambda^2+1}}-2\right)}{5\sqrt{\frac{1}{\lambda^2+1}}-6}, \quad (112)$$

we plot this radius in the Fig. 18. Note that for $\lambda = 0$ we get the result of Schwarzschild. This decrease in r_{ISCO} implies a disk of massive matter closer to the event horizon. Note that
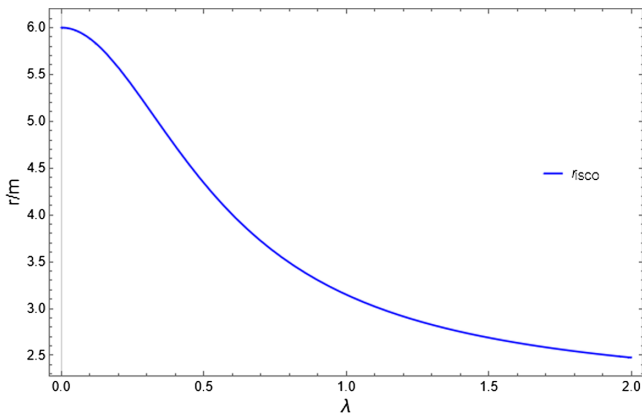

FIG. 18. Radius of the massive particle surface as function of the holonomy parameter λ given by the Eq. (112).

by defining the surfaces of photons and particles, we can construct the shadow and optical appearance of the black hole. However, we will address this issue in a later article.

VII. SUMMARY AND DISCUSSION

In this article we describe the gravitational lensing effect for the Schwarzschild solution with holonomy corrections. We treat the effect using the two types of limits commonly treated in the literature, i.e., the weak and the strong field regimes. Our main goal was to measure the influence of the parameter λ associated with loop quantum gravity on the deflection angle and observables for each regime. We have used the method described by Keeton and Petters [73], where α is approximated by a power series around u/m. And for the strong field we use the formalism proposed by Bozza [58], where the deflection angle is given by a logarithmic approximation.

More specifically, in Sec. II we explored with the weak field regime, in which the formalism was summarized and applied it to the Schwarzschild solution, where the first term of the expansion, $\mathcal{A}_1 = 4$, reduces to Einstein's result [79]. Furthermore, we applied the formalism to the modified solution and found the expansion for the deflection angle in powers up to the order of $(m/u)^5$. An interesting detail is that the first order coefficient is different from four, i.e., $\mathcal{A}_1 \neq 4$, highlighting the fact that we are not working with classical general relativity. We note that the presence of the constant λ, a parameter related to loop quantum gravity (LQG), increases the deflection angle, as can be seen from the analysis of Fig. 2. From the expression for α, we derived the expression for the image position, magnification, total magnification, and position of the centroid (observables commonly discussed in the literature). We wrote the expression for these observables as an expansion in terms of the factor $\epsilon\theta_E/4D$, where θ_E is the Einstein angle. Keeton and Petters [73] pointed out that in any hypothesis involving general relativity, the total magnification and the position of the center of gravity would not have first-order terms in this expansion, but here we can obtain these terms since $\mathcal{A}_1 \neq 4$. We show the influence of the LQG parameter on the observables in the Figs. 3–6.

Section III was devoted to the proof that the coefficient $\mathcal{A}_1$ can be determined by a method other than the geodesic one. As described in [81], the Gauss-Bonnet theorem reduces to the expression (43) in the case of gravitational lensing. We started from the same metric we used in the previous treatment and obtained the so-called optical metric and used it to calculate the Gaussian curvature K. As in the previous method, the integrals involved are not exactly solvable. We first used a Taylor series expansion that considers up to order λ^2 (50) and later up to first order m/u (52). This gave us exactly the same coefficient that we found earlier. It is interesting to note that this method leads to coefficients of higher order than the first, which are

different from Eq. (23). This is a point we would like to investigate in a future paper.

In Sec. IV, we addressed the strong field limit. As in the weak field regime, we began with a brief definition of the formalism used to obtain the approximation to this regime. We showed that the expression (55), which holds for any static and spherically symmetric metric, is an approximation of the deflection angle when $x_0 \to x_m$ (where x_0 is the distance of closest approach and x_m is the capture radius or the radius of the photon sphere), or in terms of the impact parameter $u \to u_m$. We applied the formalism to the Schwarzschild solution ($x_m = 1.5$) and showed in Fig. 7 the exact deflection angle [obtained by numerical integration of (6)] and the approximations for weak and strong fields for this solution. We then applied the formalism to the Schwarzschild solution with holonomy corrections. The radius of the photon sphere is the same as the previous one since it does not depend on the metric function $B(r)$, therefore, u_m will also be the same. The coefficient b_1 (86) can be obtained easily, however, the integral (88) cannot be evaluated to zero for any value of the parameter λ. Therefore, we computed the coefficient b_2 numerically using the interval $0 < \lambda < 2$. Figure 8 showed the variation of the coefficients as a function of the LQG parameter. In Figs. 9–11 we showed the behavior of the deflection angle with respect to λ. We verified that, as in the weak-field regime, it increases with increasing parameter.

In Sec. V we calculate the observables using a numerical example with experimental data of the black hole at the center of our galaxy (Sagittarius A*) [83–85]. For the weak field regime, we focus on a situation with two images, one with positive parity and the other with negative parity. The observables in this case are the angular separation P_t, the difference in angular positions ΔP, the total flux F_t, the flux difference ΔF, the centroid Θ_{cent}, and the differential time delay $\Delta \tau$. Figures 12–17 show a plot of these quantities as a function of the angle of the source β and the LQG parameter. We see that the influence of λ on these quantities is small. For the strong field regime, we focus on the asymptotic position approached by a set of images ϑ_∞, the distance between the first image (denoted ϑ_1) and the other s, the ratio between the flux of the first image and the flux of all other images r_m, and on the time delay between a photon with 2 loops and a photon with one loop around the lens $\Delta T_{2,1}$. We find that the observable ϑ_∞ does not depend on λ, s and $\Delta T_{2,1}$ increase with it, while r_m decreases. We showed in Table I the numerical result obtained. There are already attempts to measure the strong gravitational lensing effect [65]. We therefore hope that in the near future it will be possible to use this formalism to select a particular model of a black hole via the coefficients of the strong field.

In Sec. VI we have considered the extension of the concept of photon surface described in [86] and applied it to the corrected Schwarzschild solution. We determined the radius of the innermost stable circular orbit (ISCO) and found that it decreases with increasing parameter λ. This form of obtaining particle surfaces with the same properties as the photon sphere may be of interest in a future work where we plan to address the shadows of this solution.

[1] J. Stachel e R. Penrose, *Einstein's Miraculous Year: Five Papers That Changed the Face of Physics* (Princeton University Press, Nova Jersey, 2005).

[2] K. Schwarzschild, Über das Gravitationsfeld eines Massenpunktes nach der Einsteinschen Theorie, Sitzungsberichte der Königlich Preußischen Akademie der Wissenschaften **1916**, 189 (1916).

[3] C. A. R. Herdeiro and J. P. S. Lemos, The black hole fifty years after: Genesis of the name, arXiv:1811.06587.

[4] K. Akiyama *et al.* (Event Horizon Telescope Collaboration), First M87 event horizon telescope results. I. The shadow of the supermassive black hole, Astrophys. J. **875,** L1 (2019).

[5] K. Akiyama *et al.* (Event Horizon Telescope Collaboration), First M87 event horizon telescope results. II. Array and instrumentation, Astrophys. J. Lett. **875,** L2 (2019).

[6] K. Akiyama *et al.* (Event Horizon Telescope Collaboration), First M87 event horizon telescope results. III. Data processing and calibration, Astrophys. J. Lett. **875,** L3 (2019).

[7] K. Akiyama *et al.* (Event Horizon Telescope Collaboration), First M87 event horizon telescope results. IV. Imaging the

central supermassive black hole, Astrophys. J. Lett. **875,** L4 (2019).

[8] K. Akiyama *et al.* (Event Horizon Telescope Collaboration), First M87 event horizon telescope results. V. Physical origin of the asymmetric ring, Astrophys. J. Lett. **875,** L5 (2019).

[9] K. Akiyama *et al.* (Event Horizon Telescope Collaboration), First M87 event horizon telescope results. VI. The shadow and mass of the central black hole, Astrophys. J. Lett. **875,** L5 (2019).

[10] H. Stephani, D. Kramer, M. MacCallum, C. Hoenselaers, and E. Herlt, *Exact Solutions of Einstein's Field Equations*, 2nd ed., Cambridge Monographs on Mathematical Physics (Cambridge University Press, Cambridge, England, 2003).

[11] S. W. Hawking and G. F. R. Ellis, *The Large Scale Structure of Space-Time* (Cambridge University Press, Cambridge, England, 2023).

[12] G. J. Olmo, D. Rubiera-Garcia, and A. Sanchez-Puente, Accelerated observers and the notion of singular spacetime, Classical Quantum Gravity **35,** 055010 (2018).

[13] B. S. DeWitt, Quantum Theory of Gravity. I. The Canonical Theory, Phys. Rev. **160,** 1113 (1967).

[14] A. Ashtekar and E. Bianchi, A short review of loop quantum gravity, Rep. Prog. Phys. **84,** 042001 (2021).

[15] T. Thiemann, Modern canonical quantum general relativity, arXiv:gr-qc/0110034.

[16] R. Percacci, Gravity as a quantum field theory, Symmetry **15,** 449 (2023).

[17] J. F. Donoghue, General relativity as an effective field theory: The leading quantum corrections, Phys. Rev. D **50,** 3874 (1994).

[18] C. P. Burgess, Quantum gravity in everyday life: General relativity as an effective field theory, Living Rev. Relativity **7,** 5 (2004).

[19] I. L. Buchbinder, S. D. Odintsov, and I. L. Shapiro, *Effective Action in Quantum Gravity*, Routledge, Taylor and Francisco Group (CRC Press, Boca Raton, Florida, 1992).

[20] L. I. Bevilaqua, A. C. Lehum, and H. Souza, Universality of gauge coupling constant in the Einstein-QED system, Phys. Rev. D **104,** 125019 (2021).

[21] L. I. Bevilaqua, M. Dias, A. C. Lehum, C. R. Senise, Jr., A. J. da Silva, and H. Souza, Gravitational corrections to two-loop beta function in quantum electrodynamics, Phys. Rev. D **104,** 125001 (2021).

[22] H. Souza, L. Ibiapina Bevilaqua, and A. C. Lehum, Gravitational corrections to a non-Abelian gauge theory, Phys. Rev. D **106,** 045010 (2022).

[23] H. Souza, L. Ibiapina Bevilaqua, and A. C. Lehum, Gravitational corrections to the Einstein-scalar-QCD model, Phys. Rev. D **107,** 125012 (2023).

[24] X. Calmet and S. K. Majee, Effective theory for dark matter and a new force in the dark matter sector, Phys. Lett. B **679,** 267 (2009).

[25] X. Calmet and F. Kuipers, Implications of quantum gravity for dark matter, Int. J. Mod. Phys. D **30,** 2142004 (2021).

[26] M. Bojowald, Absence of singularity in loop quantum cosmology, Phys. Rev. Lett. **86,** 5227 (2001).

[27] S. Saini and P. Singh, Generic absence of strong singularities and geodesic completeness in modified loop quantum

cosmologies, Classical Quantum Gravity **36,** 105014 (2019).

[28] S. Saini and P. Singh, Generic absence of strong singularities in loop quantum Bianchi-IX spacetimes, Classical Quantum Gravity **35,** 065014 (2018).

[29] A. Ashtekar, T. Pawlowski, and P. Singh, Quantum nature of the big bang: Improved dynamics, Phys. Rev. D **74,** 084003 (2006).

[30] M. Varadarajan, On the resolution of the big bang singularity in isotropic loop quantum cosmology, Classical Quantum Gravity **26,** 085006 (2009).

[31] M. Bojowald, Loop quantum cosmology, Living Rev. Relativity **8,** 11 (2005).

[32] A. Ashtekar and P. Singh, Loop quantum cosmology: A status report, Classical Quantum Gravity **28,** 213001 (2011).

[33] A. Ashtekar, J. Baez, A. Corichi, and K. Krasnov, Quantum geometry and black hole entropy, Phys. Rev. Lett. **80,** 904 (1998).

[34] B. Vakili, Classical polymerization of the Schwarzschild metric, Adv. High Energy Phys. **2018,** 3610543 (2018).

[35] C. G. Boehmer and K. Vandersloot, Loop quantum dynamics of the Schwarzschild interior, Phys. Rev. D **76,** 104030 (2007).

[36] D. W. Chiou, Phenomenological loop quantum geometry of the Schwarzschild black hole, Phys. Rev. D **78,** 064040 (2008).

[37] J. Ben Achour, F. Lamy, H. Liu, and K. Noui, Polymer Schwarzschild black hole: An effective metric, Europhys. Lett. **123,** 20006 (2018).

[38] N. Bodendorfer, F. M. Mele, and J. Münch, Effective quantum extended spacetime of polymer Schwarzschild black hole, Classical Quantum Gravity **36,** 195015 (2019).

[39] A. Alonso-Bardaji, D. Brizuela, and R. Vera, An effective model for the quantum Schwarzschild black hole, Phys. Lett. B **829,** 137075 (2022).

[40] A. Alonso-Bardaji, D. Brizuela, and R. Vera, Nonsingular spherically symmetric black-hole model with holonomy corrections, Phys. Rev. D **106,** 024035 (2022).

[41] Z. S. Moreira, H. C. D. Lima, Junior, L. C. B. Crispino, and C. A. R. Herdeiro, Quasinormal modes of a holonomy corrected Schwarzschild black hole, Phys. Rev. D **107,** 104016 (2023).

[42] F. Dyson, A. Eddington, and C. Davidson, A determination of the deflection of light by the Sun's gravitational field, from observations made at the total eclipse of May 29, 1919, Philos. Trans. R. Soc. London **220,** 291 (1920).

[43] L. C. B. Crispino and D. J. Kennefick, A hundred years of the first experimental test of general relativity, Nat. Phys. **15,** 416 (2019).

[44] Arthur B. Congdon and Charles R. Keeton, *Principles of Gravitational Lensing: Light Deflection as a Probe of Astrophysics and Cosmology* (Springer, New York, 2018).

[45] R. Kayser, T. Schramm, and L. Nieser, Gravitational lenses, *Proceedings of a Conference in Hamburg, Germany* (Springer, New York City, 1991).

[46] K. S. Virbhadra and G. F. R. Ellis, Schwarzschild black hole lensing, Phys. Rev. D **62,** 084003 (2000).

[47] C. M. Claudel, K. S. Virbhadra, and G. F. R. Ellis, The geometry of photon surfaces, J. Math. Phys. (N.Y.) **42**, 818 (2001).

[48] A. G. Riess *et al.* (Supernova Search Team), Observational evidence from supernovae for an accelerating universe and a cosmological constant, Astron. J. **116**, 1009 (1998).

[49] S. Perlmutter *et al.* (Supernova Cosmology Project Collaboration), Measurements of Ω and Λ from 42 high redshift supernovae, Astrophys. J. **517**, 565 (1999).

[50] E. J. Copeland, M. Sami, and S. Tsujikawa, Dynamics of dark energy, Int. J. Mod. Phys. D **15**, 1753 (2006).

[51] J. Prat *et al.* (DES Collaboration), Dark energy survey year 1 results: Galaxy-galaxy lensing, Phys. Rev. D **98**, 042005 (2018).

[52] J. Frieman, M. Turner, and D. Huterer, Dark energy and the accelerating universe, Annu. Rev. Astron. Astrophys. **46**, 385 (2008).

[53] M. Bartelmann and P. Schneider, Weak gravitational lensing, Phys. Rep. **340**, 291 (2001).

[54] D. E. Holz and R. M. Wald, A new method for determining cumulative gravitational lensing effects in inhomogeneous universes, Phys. Rev. D **58**, 063501 (1998).

[55] A. Lewis and A. Challinor, Weak gravitational lensing of the CMB, Phys. Rep. **429**, 1 (2006).

[56] H. Ghaffarnejad and H. Niad, Weak gravitational lensing from regular Bardeen black holes, Int. J. Theor. Phys. **55**, 1492 (2016).

[57] D. H. Weinberg, M. J. Mortonson, D. J. Eisenstein, C. Hirata, A. G. Riess, and E. Rozo, Observational probes of cosmic acceleration, Phys. Rep. **530**, 87 (2013).

[58] V. Bozza, Gravitational lensing in the strong field limit, Phys. Rev. D **66**, 103001 (2002).

[59] V. Bozza and L. Mancini, Observing gravitational lensing effects by Sgr A* with GRAVITY, Astrophys. J. **753**, 56 (2012).

[60] S. Pietroni and V. Bozza, The impact of gravitational lensing in the reconstruction of stellar orbits around Sgr A*, J. Cosmol. Astropart. Phys. 12 (2022) 018.

[61] N. Tsukamoto, Deflection angle of a light ray reflected by a general marginally unstable photon sphere in a strong deflection limit, Phys. Rev. D **102**, 104029 (2020).

[62] N. Tsukamoto, Gravitational lensing in the Simpson-Visser black-bounce spacetime in a strong deflection limit, Phys. Rev. D **103**, 024033 (2021).

[63] N. Tsukamoto, Gravitational lensing by a photon sphere in a Reissner-Nordström naked singularity spacetime in strong deflection limits, Phys. Rev. D **104**, 124016 (2021).

[64] J. Zhang and Y. Xie, Gravitational lensing by a black-bounce-Reissner–Nordström spacetime, Eur. Phys. J. C **82**, 471 (2022).

[65] J. W. Nightingale, R. J. Smith, Q. He, C. M. O'Riordan, J. A. Kegerreis, A. Amvrosiadis, A. C. Edge, A. Etherington, R. G. Hayes, A. Kelly *et al.*, Abell 1201: Detection of an ultramassive black hole in a strong gravitational lens, Mon. Not. R. Astron. Soc. **521**, 3298 (2023).

[66] R. Legin, Y. Hezaveh, L. Perreault-Levasseur, and B. Wandelt, A framework for obtaining accurate posteriors of strong gravitational lensing parameters with flexible priors and implicit likelihoods using density estimation, Astrophys. J. **943**, 4 (2023).

[67] J. Wambsganss, Discovering galactic planets by gravitational microlensing: magnification patterns and light curves, Mon. Not. R. Astron. Soc. **284**, 172 (1997).

[68] V. Bozza, E. Bachelet, F. Bartolić, T. Heintz, A. Hoag, and M. Hundertmark, VBBinaryLensing: A public package for microlensing light curve computation, Mon. Not. R. Astron. Soc. **479**, 5157 (2018).

[69] S. Sajadian and K. C. Sahu, Detecting isolated stellar-mass black holes with the Roman telescope, Astron. J. **165**, 96 (2023).

[70] I. G. Shin, C. Han, A. Gould, A. Udalski, T. Sumi, M. Dominik, J. P. Beaulieu, Y. Tsapras, V. Bozza, M. K. Szymanski *et al.*, Microlensing binaries with brown dwarf companions, Astrophys. J. **760**, 116 (2012).

[71] J. Y. Choi, C. Han, A. Udalski, T. Sumi, B. S. Gaudi, A. Gould, D. P. Bennett, M. Dominik, J. P. Beaulieu, Y. Tsapras *et al.*, Microlensing discovery of a population of very tight, very low-mass binary brown dwarfs, Astrophys. J. **768**, 129 (2013).

[72] V. Bozza and L. Mancini, Time delay in black hole gravitational lensing as a distance estimator, Gen. Relativ. Gravit. **36**, 435 (2004).

[73] C. R. Keeton and A. O. Petters, Formalism for testing theories of gravity using lensing by compact objects. I. Static, spherically symmetric case, Phys. Rev. D **72**, 104006 (2005).

[74] C. R. Keeton and A. O. Petters, Formalism for testing theories of gravity using lensing by compact objects. II. Probing post-post-Newtonian metrics, Phys. Rev. D **73**, 044024 (2006).

[75] C. R. Keeton and A. O. Petters, Formalism for testing theories of gravity using lensing by compact objects. III. Braneworld gravity, Phys. Rev. D **73**, 104032 (2006).

[76] Z. Horvath, L. A. Gergely, Z. Keresztes, T. Harko, and F. S. N. Lobo, Constraining Hořava-Lifshitz gravity by weak and strong gravitational lensing, Phys. Rev. D **84**, 083006 (2011).

[77] A. Kehagias and K. Sfetsos, The black hole and FRW geometries of non-relativistic gravity, Phys. Lett. B **678**, 123 (2009).

[78] T. K. Poddar, Constraints on axionic fuzzy dark matter from light bending and Shapiro time delay, J. Cosmol. Astropart. Phys. 09 (2021) 041.

[79] S. Weinberg, *Gravitation and Cosmology: Principles and Applications of the General Theory of Relativity* (Wiley, New York, 1972).

[80] R. F. Lukmanova, G. Y. Tuleganova, R. N. Izmailov, and K. K. Nandi, Lensing observables: Massless dyonic vis-à-vis Ellis wormholes, Phys. Rev. D **97**, 124027 (2018).

[81] G. W. Gibbons and M. C. Werner, Applications of the Gauss-Bonnet theorem to gravitational lensing, Classical Quantum Gravity **25**, 235009 (2008).

[82] Z. Li and T. Zhou, Equivalence of Gibbons-Werner method to geodesics method in the study of gravitational lensing, Phys. Rev. D **101**, 044043 (2020).

[83] D. Richstone, E. A. Ajhar, R. Bender, G. Bower, A. Dressler, S. M. Faber, A. V. Filippenko, K. Gebhardt, R. Green, L. C. Ho *et al.*, Supermassive black holes and the evolution of galaxies, Nature (London) **395,** A14 (1998).

[84] K. Akiyama *et al.* (Event Horizon Telescope Collaboration), First Sagittarius A* event horizon telescope results. I. The shadow of the supermassive black hole in the center of the Milky Way, Astrophys. J. Lett. **930,** L12 (2022).

[85] R. Abuter *et al.* (GRAVITY Collaboration), Polarimetry and astrometry of NIR flares as event horizon scale, dynamical probes for the mass of Sgr A*, arXiv:2307.11821.

[86] K. Kobialko, I. Bogush, and D. Gal'tsov, Geometry of massive particle surfaces, Phys. Rev. D **106,** 084032 (2022).